ICAS-98-R,3,11

A98-31575

THREE DIMENSIONAL FLOW SIMULATION IN THE TEST SECTION OF A SLOTTED TRANSONIC WIND TUNNEL

Renato Vieira*
Faculdade de Engenharia de Guaratinguetá
UNESP/FEG
12500-000 – Guaratinguetá – SP – BRAZIL

João Luiz F. Azevedo†
Instituto de Aeronáutica e Espaço
CTA/IAE/ASE-N
12228-904 – São José dos Campos – SP – BRAZIL

Nide G.C.R. Fico Jr.‡, Edson Basso§
Instituto Tecnológico de Aeronáutica
CTA/ITA/IEAA
12228-900 – São José dos Campos – SP – BRAZIL

Abstract

The paper presents flow simulations relevant to transonic wind tunnel design and operation. A three-dimensional, finite difference, computational code which solves the Euler equations in a general, body conforming, curvilinear grid has been developed and used for these simulations. This code incorporates the capability of including test section wall slots for realistic simulation of a transonic wind tunnel facility. Test cases considered include a tunnel contraction alone and a complete high speed tunnel segment. Both cases with closed and open slots were considered. The results obtained adequately reproduced the expected flow features for the conditions analyzed and indicated that the particular configuration studied holds promise of providing very good test section flow quality.

Introduction

The present work is concerned with developing the capability of simulating flowfields relevant to transonic wind tunnel applications. Centro Técnico Aeroespacial (CTA) is in the process of designing a production transonic wind tunnel facility. The complete facility being designed at CTA has a 2.0 × 2.4 m test section. Clearly, the costs involved in such enterprise are very large. To minimize the technical risks involved, the project's first phase consists of the construction and operation of a reduced scale pilot tunnel, called the TTP facility. The TTP is currently being built and the authors involvement has been in the simulation of flows in this pilot facility.

Computational Fluid Dynamics (CFD) methods are enjoying increasing application assisting in the selection of tunnel airline component geometry[1]. These techniques have been used to design diffusers and flexible nozzles as well as to investigate other aspects of the tunnel flow. Transonic wind tunnels usually operate from low subsonic Mach numbers ($M \cong 0.25$) to the supersonic regime ($M \cong 1.6$). The tunnel nozzle is a key element in achieving the desired test-section Mach number, M_{TS}. Hence, previous work by some of the present authors[2] has concentrated in flow simulations for the tunnel contraction. The present effort intended to build upon such experience in order to include the tunnel test section and the effect of the wall slots.

It is well known that transonic tunnel test sections must have ventilated, either slotted or perforated, walls. CTA has decided to use slotted walls. In this context, one of the major interests in using CFD simulations is to aid in the assurance of good test section flow quality. Clearly, this is closely related to the shape of the slots as well as to the open area ratio, among other parameters. Therefore, one could state that the major objective of the present work was to study, using CFD techniques, flowfields which are relevant for the TTP design and operation. This has the long term goal of developing reliable computational tools that could be used for flow simulation inside transonic wind tunnel facilities, including the effect of ventilated walls.

The work briefly describes the main aspects of test-section mass extraction, the formulation of the codes

*Undergraduate Student.
†Head, Aeroelasticity & CFD Sections, Space Systems Division.
‡Professor, Aerodynamics Department.
§Graduate Student.

21st ICAS Congress
13-18 September 1998
Melbourne, Australia

used and concentrates on the discussion of the results obtained so far. Limitations observed in the algorithms which were used for the previous work[2] motivated the development of a completely new three dimensional code. Hence, the initial simulations considered again the tunnel contraction alone. These calculations were used to validate the new implementation, based on the results previously available. Afterwards, the tunnel test section was included in the computational domain and simulations were performed both with and without ventilated walls. Clearly, in the actual operating conditions, the slots are present in the test section and some mass extraction is necessary in order to maintain good test section flow quality. However, the non-porous wall is a limiting case which is also interesting to be tested in the code validation process. In the ventilated wall cases, the amount of mass extracted through the slots is controlled by the specified plenum chamber pressure. This parameter was varied to cover the complete range of interest in terms of test-section mass extraction values.

Mass Extraction

In this section, the main implications of test section mass extraction are highlighted. The tunnel test section is supposed empty and its walls are parallel. There are three basic ways[3] of extracting mass through the test section walls: *(i)* flap evacuation, *(ii)* evacuation using auxiliary compressors (forced evacuation) and *(iii)* mixed evacuation, which is uses both the flaps and the auxiliary compressors. In the present work, the actual mass extraction mechanism is irrelevant as the computational domain is restricted to the test section itself. In other words, it does not extend to the flap region just at the difuser entrance. Moreover, the plenum chamber is not being modeled in this phase of the work. The effect of the plenum chamber is represented by the pressure boundary condition at the slots. The lower this pressure, the larger the amount of mass which would be extracted by the auxiliary compressors.

A continuous variation of the Mach number, in the transonic range, can be obtained using a sonic contraction and performing mass extraction at the test section. The Mach number is controlled by the amount of mass being evacuated from the test section to plenum chamber that surrounds it. This type of setup is, of course, limited in the sense that for M_{TS} greater than 1.27 the amount of mass one has to extract at the test section becomes prohibitive. In such cases it is wise to equip the closed circuit wind tunnel with a Laval nozzle.

The high-speed section of the tunnel extends from the contraction to the difuser entrance. Once this geometry is fixed, the Mach number distribution along the test section is determined by the main compressor pressure ratio, λ_c, and the percentage of mass extraction $\dot{m}_s/\dot{m}$. Here, $\dot{m}_s$ is the extracted mass and $\dot{m}$ is the tunnel total mass. There are many combinations of λ_c and $\dot{m}_s/\dot{m}$ that will yield the desired test section Mach number. However, only one of these will provide an *uniform* M_{TS} distribution over the entire test section length. This particular combination is the so-called *optimum suction*.

Figure 1 shows, for M_{TS}, how the the mass extraction relates to the main compressor pressure ratio and to the test section flow quality. For $M_{TS} = 1.2$, several combinations of the pair λ_c and $\dot{m}_s/\dot{m}$, numbered 1 to 5, are shown. Each of these yield a different Mach number at the difuser entrance as well as a particular Mach number distribution along the test section length. Of all the possible pairs only one is able to supply the test section with a uniform Mach number distribution. This particular combination is marked as point 3 in Fig. 1. If the main compressor pressure ratio is increased beyond point 3, keeping the mass extraction constant, the total power to run the tunnel will augment with no actual benefits in terms of test-section flow quality. In other words, energy will be wasted. On the other hand, diminishing λ_c results in the decrease of the usable test section length and the need for a larger amount of mass extraction. Another interesting point is that the sonic nozzle demands less power[4] than the Laval nozzle at the point of optimun suction. This is due to the fact that the boundary layer thickness at the difuser entrance is slightly smaller when the tunnel is equiped with a sonic nozzle as it demands more mass extraction along the test section.

The impact of mass extraction upon the tunnel total power is shown in Fig. 2. In this case, the ratio $\dot{m}_s/\dot{m} = 2.7\%$, which is the optimun value. It is seen that there is substantial energy savings if the tunnel operates with forced evacuation. The explanation in this case is similar to the one above, that is, the boundary layer at the difuser entrance is diminished as a consequence of the mass suction along the test section, which in turn improves the difuser performance.

Theoretical Formulation

The flow simulations here reported were performed using the three-dimensional, compressible Euler equations. These equations can be written in strong conservation-law form for general, body-conforming, curvilinear coordinates[5, 6] as

$$\frac{\partial \overline{Q}}{\partial \tau} + \frac{\partial \overline{E}}{\partial \xi} + \frac{\partial \overline{F}}{\partial \eta} + \frac{\partial \overline{G}}{\partial \zeta} = 0 \,. \qquad (1)$$

The vector of conserved quantities, $\overline{Q}$, can be defined as

$$\overline{Q} = J^{-1} \left[\begin{array}{ccccc} \rho & \rho u & \rho v & \rho w & e \end{array} \right]^{\mathrm{T}} , \qquad (2)$$

and the flux vectors, $\overline{E}$, $\overline{F}$ and $\overline{G}$, can be written as

$$\overline{E} = J^{-1} \left\{ \begin{array}{c} \rho U \\ \rho u U + p \xi_x \\ \rho v U + p \xi_y \\ \rho w U + p \xi_z \\ (e+p) U - p \xi_t \end{array} \right\} , \qquad (3)$$

$$\overline{F} = J^{-1} \left\{ \begin{array}{c} \rho V \\ \rho u V + p \eta_x \\ \rho v V + p \eta_y \\ \rho w V + p \eta_z \\ (e+p) V - p \eta_t \end{array} \right\} , \qquad (4)$$

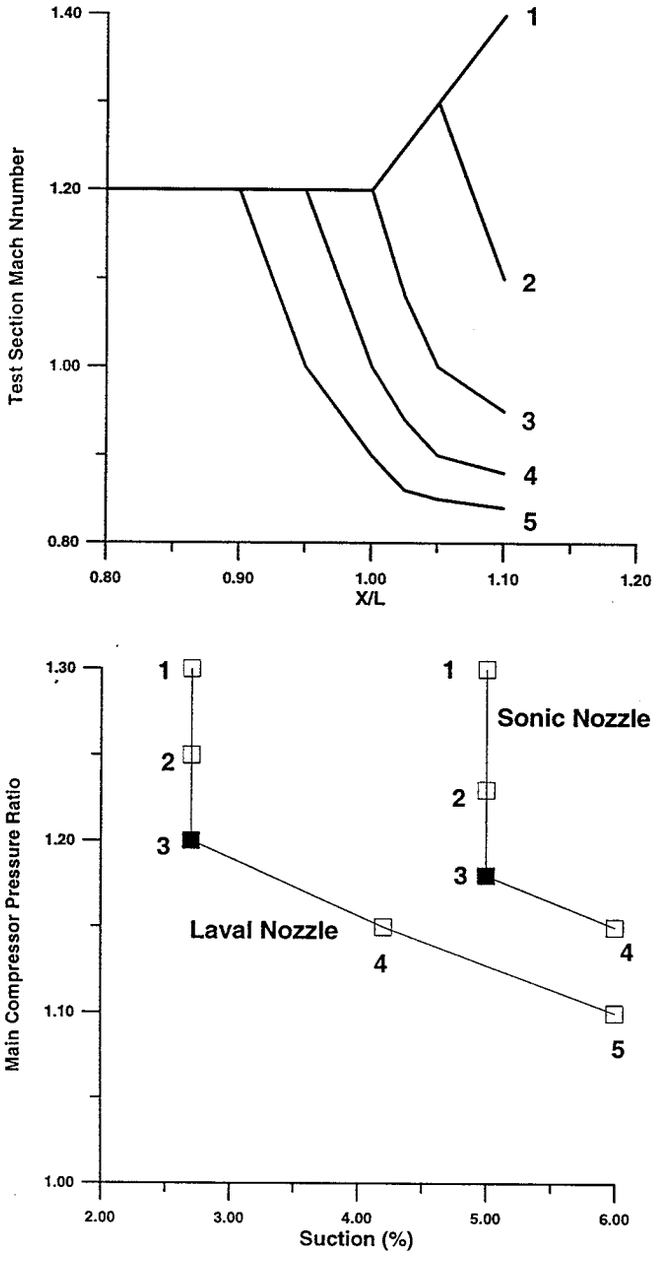

Figure 1: Illustration of the optimal suction concept.

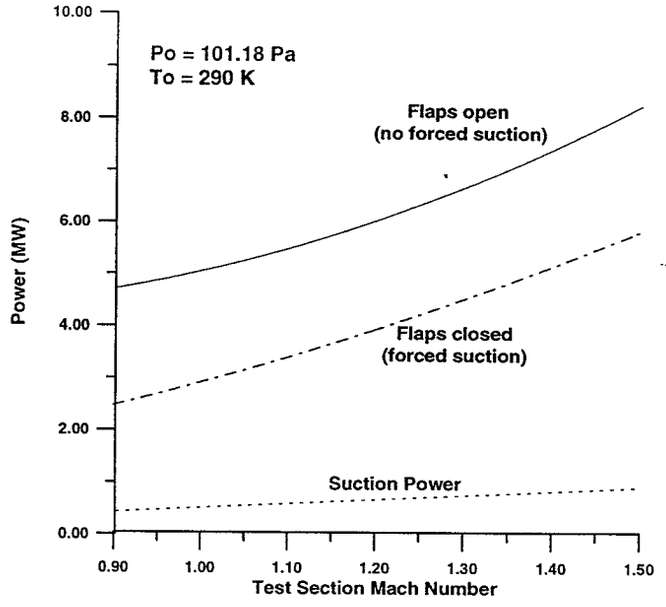

Figure 2: Comparison indicating the effect of the type of mass suction concept adopted upon the tunnel total power consumption.

$$\overline{G} = J^{-1} \begin{Bmatrix} \rho W \\ \rho u W + p\zeta_x \\ \rho v W + p\zeta_y \\ \rho w W + p\zeta_z \\ (e+p)W - p\zeta_t \end{Bmatrix} . \qquad (5)$$

The usual nomenclature is being adopted in the present case, such that ρ is the density, u, v and w are the Cartesian velocity components, p is the pressure, and e is the total energy per unit of volume. The pressure is obtained from the equation of state for perfect gases, which can be written in the present case as

$$p = (\gamma - 1)\left[e - \frac{1}{2}\rho\left(u^2 + v^2 + w^2\right)\right] , \qquad (6)$$

where γ is the ratio of specific heats. The contravariant velocity components, U, V and W, can be written as

$$\begin{aligned} U &= \xi_t + \xi_x u + \xi_y v + \xi_z w , \\ V &= \eta_t + \eta_x u + \eta_y v + \eta_z w , \\ W &= \zeta_t + \zeta_x u + \zeta_y v + \zeta_z w . \end{aligned} \qquad (7)$$

Expressions for the Jacobian of the transformation, J, and for the various metric terms can be found in Refs. [5] and [7], among other references.

Numerical Implementation

The governing equations were discretized in a finite difference context for structured hexahedral grids. The spatial discretization adopted in the present work uses

a central difference type algorithm plus explicitly added artificial dissipation terms in order to control nonlinear instabilities. The equations, fully discretized in space, can be written as

$$\left(\frac{\partial \overline{Q}}{\partial \tau}\right)_{i,j,k} = -\mathrm{RHS}_{i,j,k} \ . \qquad (8)$$

The right-hand side operator of Eq. (8) is defined as

$$\begin{aligned} \mathrm{RHS}_{i,j,k} &= \frac{1}{2\,\Delta\xi}\left(\overline{E}_{i+1,j,k} - \overline{E}_{i-1,j,k}\right) \\ &+ \frac{1}{2\,\Delta\eta}\left(\overline{F}_{i,j+1,k} - \overline{F}_{i,j-1,k}\right) \\ &+ \frac{1}{2\,\Delta\zeta}\left(\overline{G}_{i,j,k+1} - \overline{G}_{i,j,k-1}\right) \ , \qquad (9) \end{aligned}$$

where $\Delta\xi = \Delta\eta = \Delta\zeta = 1$ for the general curvilinear coordinate case. The artificial dissipation terms were implemented as described in Ref. [8].

Time march uses an explicit, 2nd-order, 5-stage Runge-Kutta scheme[9, 10], which can be written as

$$\begin{aligned} \overline{Q}^{(0)}_{i,j,k} &= \overline{Q}^{n}_{i,j,k} \ , \\ \overline{Q}^{(\ell)}_{i,j,k} &= \overline{Q}^{(0)}_{i,j,k} - \alpha_\ell \, \Delta t_{i,j,k} \, \mathrm{RHS}^{(\ell-1)}_{i,j,k} \ , \ \ell = 1, 2, \ldots, 5, \\ \overline{Q}^{n+1}_{i,j,k} &= \overline{Q}^{(5)}_{i,j,k} \ . \qquad (10) \end{aligned}$$

In the previous expressions, Δt stands for the time step, and n and $n+1$ are the properties values at the start and at the end of each time step. A variable time step convergence acceleration technique was used to accelerate convergence to steady state results. Considerable effort was invested in the accurate implementation of entrance and exit boundary conditions through the use of one-dimensional characteristic relations[11, 12].

Grid Generation

The initial simulations for the convergent-divergent nozzle were performed using a 100 × 20 × 29 point mesh, respectively in the ξ, η and ζ directions. The curvilinear coordinate system is set such that ξ is the longitudinal coordinate, η is the coordinate from the centerline to the tunnel wall, and ζ is the azimuthal direction. A typical longitudinal plane of this mesh is shown in Fig. 3. The mesh shown in Fig. 3 considers only the contraction of the tunnel, which was the configuration used for the initial simulations. When the tunnel test section was introduced in the simulations, another 50 grid points were added to the longitudinal direction. The meshes here used were all generated by algebraic methods after the data on the tunnel wall geometry was obtained from a CAD system.

The complete wind tunnel has four slots in the top and bottom test section walls, positioned at regular intervals. The tunnel lateral walls do not have the two central slots, because the space is needed for the observation windows. Therefore, the lateral walls have two slots each, located at the corresponding positions of the outer slots in the top and bottom walls. The slots have an approximate width of 5 to 6 mm. Previous experience has shown that one needs at least three computational points inside the slot width in order to obtain an adequate resolution of flow through the slots. However, the particular tunnel configuration under consideration has two symmetry planes. Therefore, one has to solve only for one-fourth of the complete tunnel, indicating that only three slots are present in the computational domain considered.

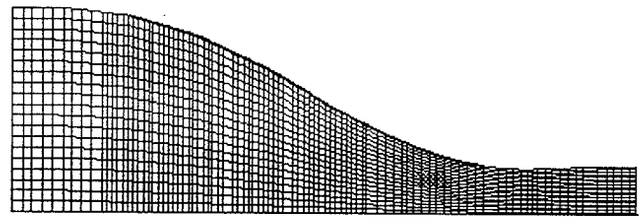

Figure 3: View of a typical longitudinal plane of the mesh for the tunnel contraction. Particular grid plane shown has 100 × 20 points.

The initial simulations with the above mesh indicated that the resolution in the ζ direction was not adequate. This experience has shown that a mesh spacing at the tunnel wall (in the azimuthal direction) of at least 5 mm was necessary, aside from further refinement at the slots themselves. This spacing would imply that 55 points were required in this direction. It must be pointed out that the ideal solution would be to have a complete refinement in the ζ direction, because this would provide a smoother mesh. However, considering that three computational points would be required within each slot and that the slots had a 5 mm width, this would imply a mesh with about 211 points in the azimuthal direction. The computational costs of a solution in such a grid, even assuming that the refinement in the other directions would remain as previously cited, were well beyond the available computational resources at the time.

Therefore, the decision adopted was to have a mesh with an average spacing at the wall in the ζ direction of approximately 5 mm and to perform a localized refinement at the slots in order to recover the necessary resolution. This mesh was generated by a linear interpolation process on the previous grid, which had 29 points in the azimuthal direction. This yielded a mesh with 55 grid points in this direction. Afterwards, and still using linear interpolation at the wall, further refinement was performed at the slots adding 12 points to the mesh. The final mesh had, therefore, 150 × 20 × 67 in the (ξ, η, ζ) directions, respectively, which provides the minimum resolution required to perform simulations with the ventilated wall wind tunnel. A typical crossflow plane of the grid in the slotted test section portion of the tunnel in shown in Fig. 4. One can clearly see in this figure the additional refinement at the slot locations and, also, some additional refinement in order to resolve the kink in the tunnel wall.

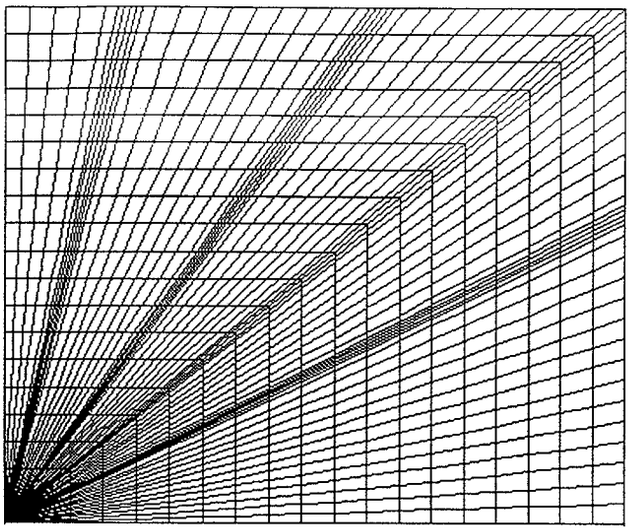

Figure 4: View of a typical crossflow plane of the mesh in the test section region, showing grid refinement at the slot locations. Crossflow grid plane shown has 20×67 points in the wall normal and azimuthal directions, respectively.

Results and Discussion

As previously discussed, the initial simulations performed considered only the tunnel contraction, i.e., the convergent-divergent nozzle portion of the tunnel. These calculations were performed with the objective of validating the code developed against results available in the literature for this configuration[2]. Moreover, there was also interest in comparing the present code computational efficiency against that provided by the previous implicit code[2]. This phase of the work used the original $100 \times 20 \times 29$ point mesh. Results for this simulation for a nominal test section Mach number, M_{TS}, of 1.3 are shown in Fig. 5. In particular, this figure presents Mach number contours along four crossflow sections at different longitudinal locations along the tunnel. The planes represent the nozzle entrance section ($i = 1$), two intermediate planes ($i = 25$ and $i = 75$) and the nozzle exit plane ($i = 100$), which corresponds to the entrance of the tunnel test section.

One can clearly observe from Fig. 5 that the Mach number variation within each crossflow section is very small, indicating a very uniform acceleration of the flow through the nozzle. The overall quality of these solutions is in very good agreement with the results reported by in Ref. [2]. The authors emphasize that the reader should pay attention to the color coding of each plot in order to observe that Mach number variations within each section are indeed very minor. Figure 6 presents the Mach number contour plots (top) and the velocity vectors (bottom) along the tunnel horizontal symmetry plane. One can observe a very uniform and smooth expansion of the flow along the nozzle. Moreover, one can also observe that the Mach contours are orthogonal to the nozzle axis and uniformly spaced along the nozzle. The conclusion that the flow

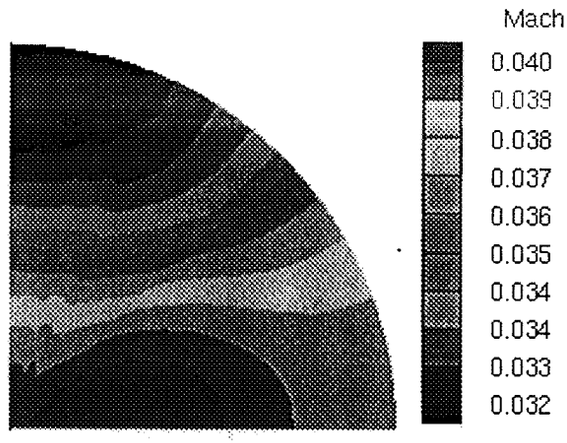

(a) Nozzle entrance plane ($i = 1$).

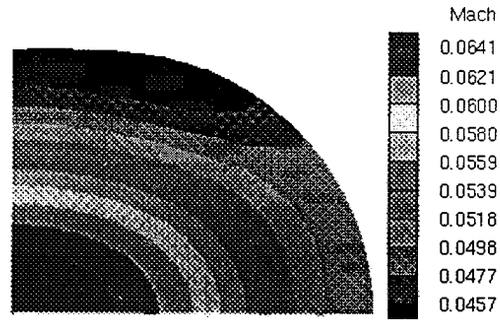

(b) Plane in the convergent portion of nozzle ($i = 25$).

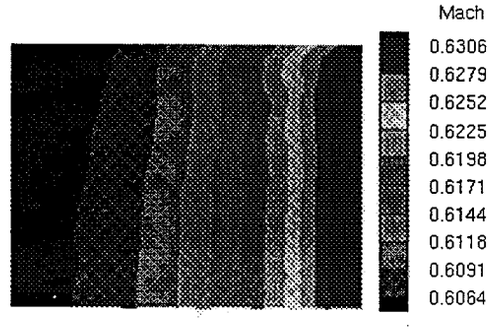

(c) Plane in the divergent portion of nozzle ($i = 75$).

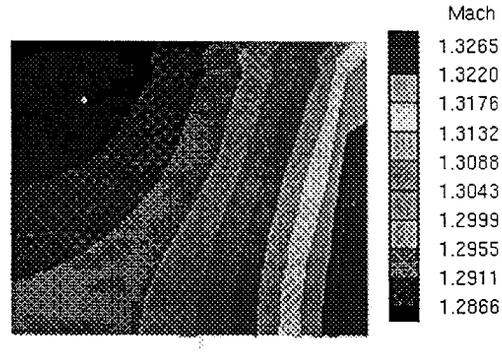

(d) Nozzle exit plane ($i = 100$).

Figure 5: Mach number contours at planes perpendicular to the nozzle axis for $M_{TS} = 1.3$.

(a) Mach number contours.

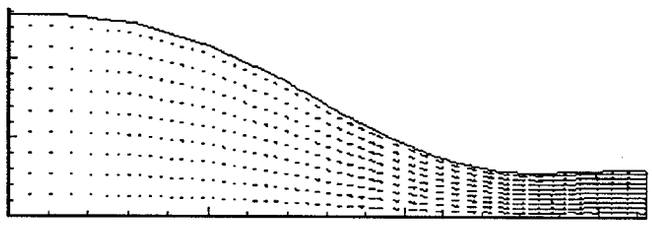

(b) Velocity vectors.

Figure 6: Solution on the nozzle horizontal symmetry plane. Simulation for the contraction alone with $M_{\mathrm{TS}} = 1.3$.

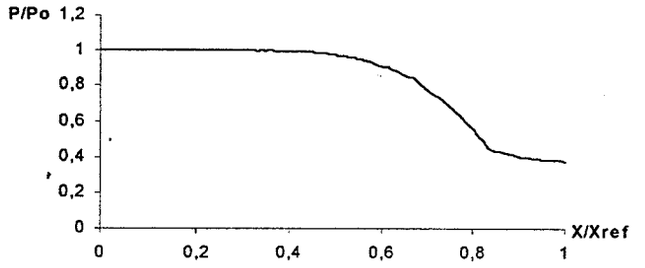

Figure 7: Wall pressure distribution in the streamwise direction for the nozzle horizontal symmetry plane. Simulation for the contraction alone with $M_{\mathrm{TS}} = 1.3$.

accelerates very smoothly along the nozzle is further emphasized by the velocity vector plot, which indicates that the flow follows the nozzle geometry without any shocks or discontinuities. Figure 7 presents the pressure distribution along the nozzle wall in the longitudinal direction for the vertical symmetry plane. This figure again indicates that there are no sharp variations in the pressure along the longitudinal direction, thus showing that there are no shock waves in the flowfield for this case. This is clearly the desired behavior since shock waves would degrade the flow quality for the tunnel test section.

Simulations were also performed for the tunnel including both the contraction and the test section, but without including the effect of the wall slots. This case will be denoted here as the closed slot case. The computational mesh used in these simulations is already the final grid with $150 \times 20 \times 67$ points, especially because the present solution provides the necessary initial condition for the simulation with the open slots, which will be discussed

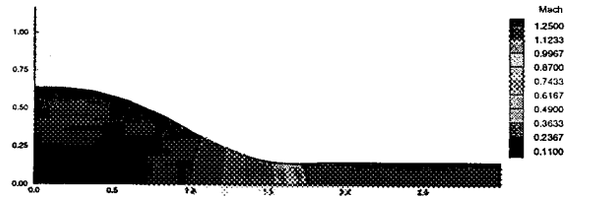

(a) Horizontal symmetry plane.

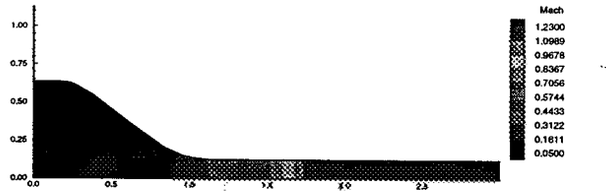

(b) Vertical symmetry plane.

Figure 8: Mach number contours in the two tunnel symmetry planes ($M_{\mathrm{TS}} = 1.3$). Due to tunnel double symmetry, only one-half of each plane is shown.

latter in the paper. An overview of the solution with the test section included in the computational domain can be seen in Fig. 8. This figure shows the Mach number distribution on the two longitudinal symmetry planes for the case of nominal test section Mach number of 1.3. The top plot in Fig. 8 is showing the horizontal symmetry plane whereas the bottom plot is showing the vertical symmetry plane. The authors emphasize that only one-half of each plane is shown, due to the tunnel double symmetry. It is clear from both plots in Fig. 8 that the Mach number is fairly constant throughout the total length of the tunnel test section.

Figure 9 presents the Mach number contours at four crossflow planes for the same case of nominal test section Mach number, M_{TS}, of 1.3. The tunnel crossflow sections represented in Fig. 9 are a plane in the upstream portion, or convergent section, of the tunnel contraction ($i = 10$), a plane in the divergent section of the nozzle ($i = 85$), the plane at the test section entrance ($i = 100$) and a plane in the downstream portion of the test section ($i = 143$). One can observe Fig. 9.(c) that the tunnel nozzle is providing a very uniform flow to the test section. Moreover, it is also fulfilling its design objective which was to provide, in this case, the tunnel test section with a $M = 1.3$ flow. Furthermore, if one compares the two bottom plots in Fig. 9, it is clear that test section Mach number variations about the nominal value of 1.3, throughout the entire test section, are extremely small. This indicates that, despite the fact that the test section is fairly long, its Mach number remains essentially constant. A similar conclusion could be reached by analyzing the pressure distribution in the test section. The pressure results are not shown here for the sake of brevity.

The forthcoming discussion considers the case of open slots for a nominal test section Mach number of 1.3. The basic boundary condition imposed at the slots is a fixed

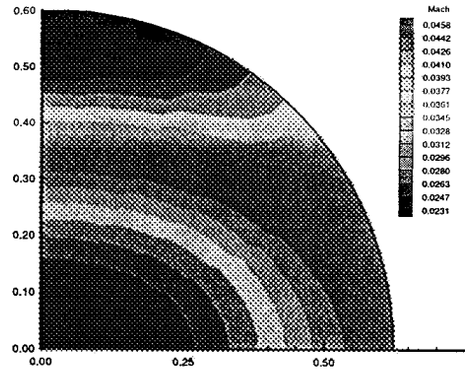

(a) Upstream portion of contraction ($i = 10$).

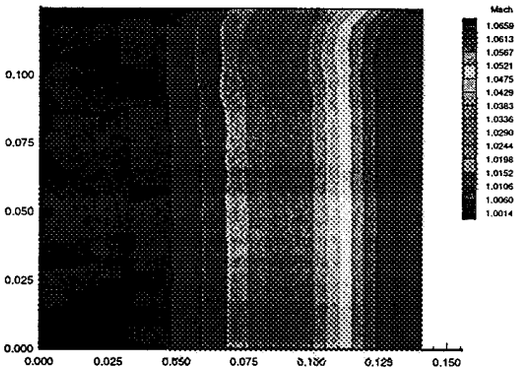

(b) Divergent section of nozzle ($i = 85$).

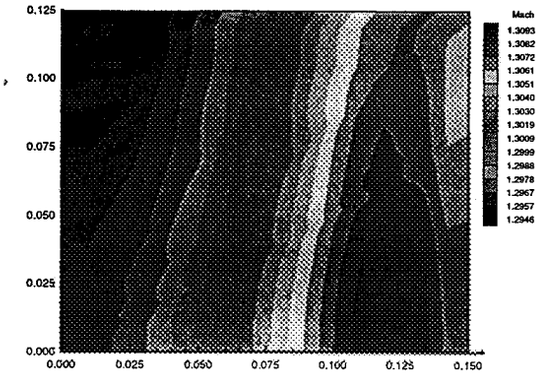

(c) Test section entrance plane ($i = 100$).

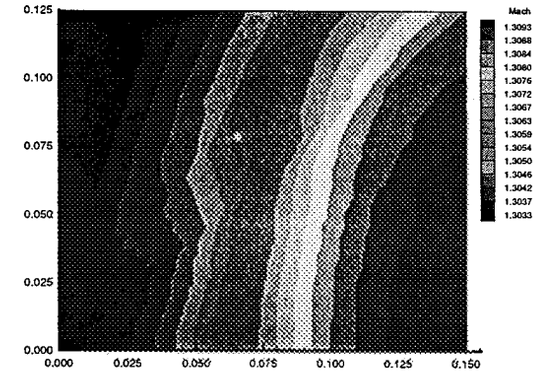

(d) Downstream portion of test section ($i = 143$).

Figure 9: Mach number contours in crossflow planes at different longitudinal positions along the tunnel for the closed slot case ($M_{TS} = 1.3$).

pressure boundary condition. This is consistent with a characteristic analysis in which the slots are treated as a subsonic exit boundary (see, for instance, Refs. [13] and [14] for more details on the use of characteristic relations for boundary condition enforcement for the Euler equations). The static pressure imposed at the slots was varied between 60 and 97% of the average static pressure at the test section entrance, i.e., plane $i = 100$, obtained from the simulation with closed slots. It should be emphasized that this is a somewhat artificial form of enforcing the slot boundary conditions because what one usually regulates in these facilities is the percentage of mass flow extracted from the test section. However, this would require the inclusion of the plenum chamber in the simulations, which is still a future step in the present development process. Therefore, the approach adopted in the present case is to impose the slot pressure and to compute the extracted mass flow as a result of the simulation. By varying the slot pressure, one can obtain the correct mass flow ratio and, hence, validate the simulations.

As an example of the results obtained in the open slot case, Fig. 10 presents the pressure distribution along the crossflow plane $i = 107$, for three instances along the numerical convergence process, for a slot static pressure equal to 95% of the average pressure at the test section entrance. This crossflow plane corresponds to the second computational plane (in the longitudinal direction) in the slotted portion of the test section. The top plot in Fig. 10 presents the section pressure distribution with the slots closed, the figure in the middle represents an instant of time just after the slots were opened, and the bottom figure is the converged solution for that section with open slots. It should be, again, emphasized that, for example, the top figure may give a false impression of wild pressure variations in this particular section. However, if one observes the figure color coding, it becomes clear that the section pressure distribution is extremely uniform with an average value of 0.306. The authors point out that the quantity plotted is the dimensionless static pressure, referred to the stagnation pressure at the entrance of the tunnel contraction. The second (middle) figure shows some reduction in the pressure level throughout the section, but especially in the region closer to the upper wall which has two slots. This pressure variation within the section tends to disappear as the solution converges, and the bottom figure evidences that by showing again a very constant pressure distribution throughout the section except, obviously, in the immediate vicinity of the slots.

The behavior described for the $i = 107$ plane is representative of what is observed throughout the slotted portion of the test section. The pressure levels with the open slots are slightly lower than their corresponding values with the closed slots. Moreoveor, the pressure distribution is essentially constant along the crossflow section once the transients have died out. Clearly, the immediate vicinity of the slots show larger pressure variations. Furthermore, one also observe that the pressure decrease in the cross flow sections is accentuated as one moves

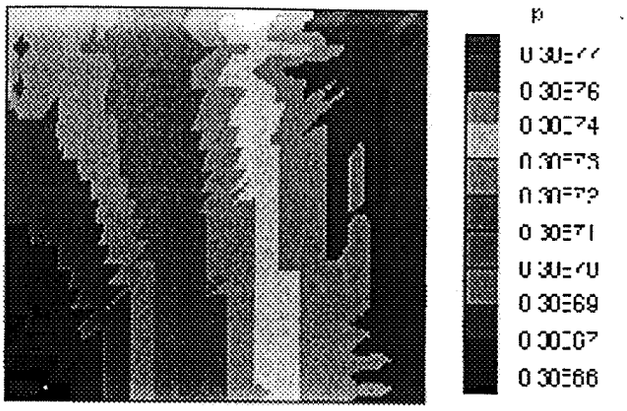

(a) Solution with closed slots.

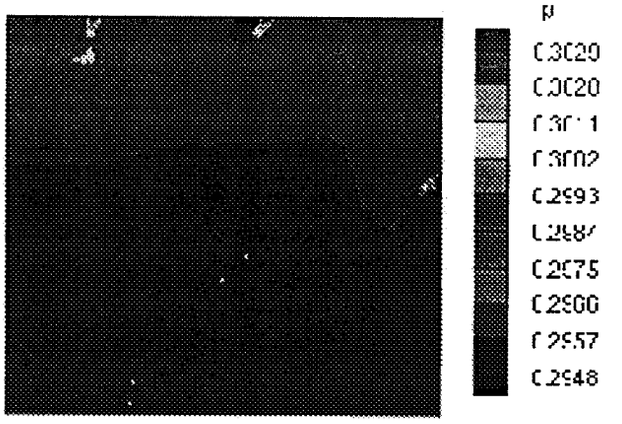

(b) Solution just after slots were opened.

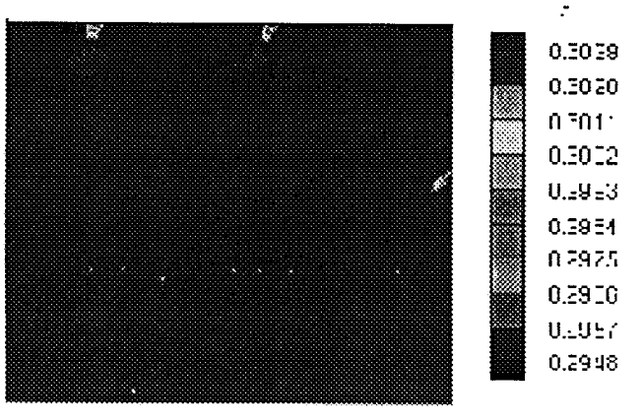

(c) Converged solution with open slots.

Figure 10: Dimensionless pressure contours at the second computational crossflow plane ($i = 107$) in the slotted portion of the test section for $M_{TS} = 1.3$ and a slot static pressure equal to 95% of the average pressure at the test section entrance.

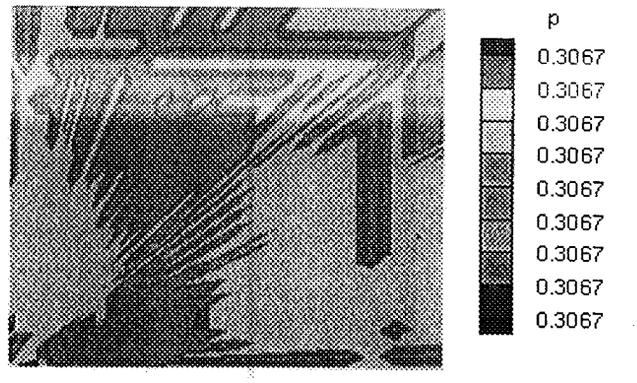

(a) Solution with closed slots.

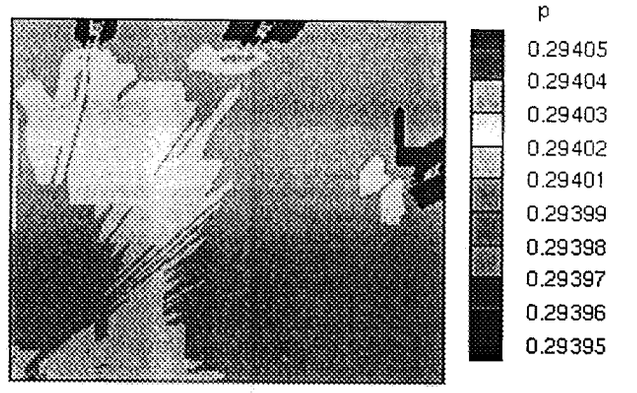

(b) Solution with open slots.

Figure 11: Dimensionless pressure contours at an intermediate plane ($i = 125$) along the tunnel test section. Results presented consider closed and open slot cases with $M_{TS} = 1.3$. The open slot case considered a slot static pressure equal to 95% of the average pressure at the test section entrance.

downstream along the tunnel test section.

As an example of the behavior described, Fig. 11 presents dimensionless pressure contours for a crossflow section halfway through the tunnel test section (i=125). The top figure presents the pressure contours with closed slots and the bottom one, the contours for the converged solution with open slots. As before, despite the rather erratic appearance of the contour colors, one can observe that there is no variation in the pressure values throughout the section up to four significative figures in the top plot. The bottom plot indicates some reduction in the section pressure level after the slots are open, but the overall behavior is very close to what has already been discussed. It should be pointed out that the behavior observed in Figs. 10 and 11 is representative of the solution in the complete tunnel test section. In general, either with closed or open slots, pressure variations within each particular section were always smaller than 0.1%, except in the immediate vicinity of the slots, thus demonstrating a high quality flow in the tunnel.

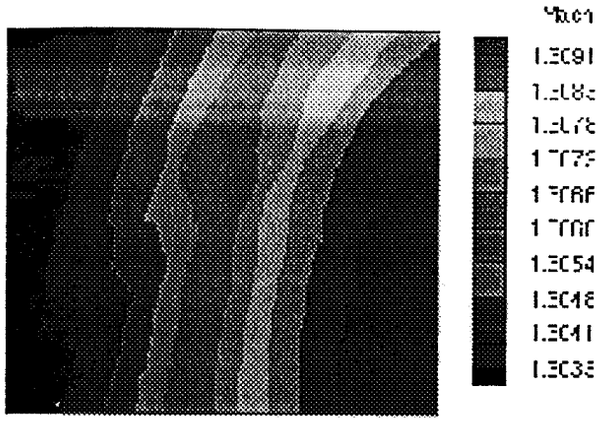

(a) Solution with closed slots.

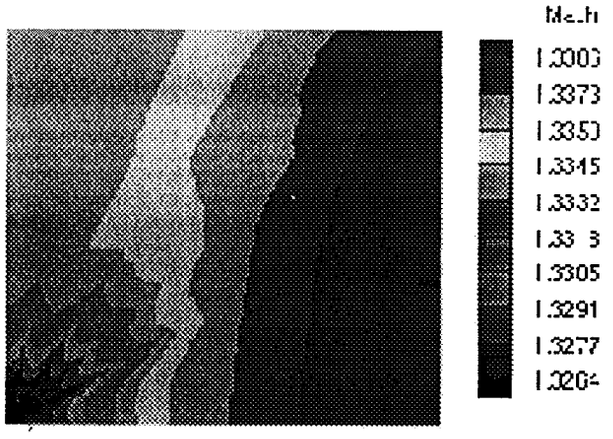

(b) Solution with open slots.

Figure 12: Mach number contours at the test section exit plane ($i = 150$) for nominal $M_{TS} = 1.3$. The open slot case considered a slot static pressure equal to 95% of the average pressure at the test section entrance.

As shown in Fig. 11, the open slots solution has a tendency of having slightly lower pressure levels as one moves downstream along the tunnel. This is the result of a certain pressure relief provided by presence of the slots. As a consequence, there is a slight increase in the flow velocity as one moves downstream along the tunnel for the open slot case. This is evidenced in Fig. 12. This figure shows the Mach number contours with closed (top) and with open (bottom) slots for the crossflow section at the tunnel exit plane ($i = 150$). One can observe that the Mach number has increased by approximately 0.03 for the open slot case, in comparison with the closed slot solution which indeed reproduces the nominal test section Mach number of 1.3. Although there is some acceleration of the flow in the open slot case, the flowfield is still very uniform within each crossflow plane. Moreover, this slight acceleration of the flow with open slots is exactly the result one should expect to find in an empty wind tunnel. Due to mass extraction through the slots, and considering that there are no viscous effects in the simulations, the test section behaves as a divergent nozzle in supersonic flow and the flow must accelerate. Furthermore, an analysis of several crossflow planes further indicates that crossflow velocities are negligible throughout the entire test section, except in the immediate vicinity of the slots.

Table 1: Percentage of mass flow extracted from the test section as a function of the slot static pressure ratio specified as boundary condition at the wall slots (nominal $M_{TS} = 1.3$).

Pressure Ratio	% of Mass Extracted
0.60	10.02
0.70	7.75
0.80	5.20
0.88	3.04
0.89	2.77
0.90	2.48
0.92	1.93
0.93	1.65
0.95	1.11
0.97	0.58

Another important aspect analyzed in the present work was an assessment of the amount of mass extracted from the tunnel main flow through the slots. As previously discussed, the slot boundary conditions adopted in the present case were somewhat artificial in the sense that one usually cannot regulate the actual pressure at the slots. The quantity actually used to exert the control over the mass extraction is amount of mass that is forced to pass through the auxiliary compressors. Clearly, this affects the pressure at the slots. Here, since the plenum chamber was not modeled in this phase of the work, the control was exercised through the specification of the plenum chamber pressure and the amount of mass extracted was a consequence of this pressure. The quantity actually specified at the slots in the present simulations was the ratio between the static pressure at the slots and the average static pressure at the test section entrance, obtained from the simulation with the slots closed. The percentage of mass flow extracted from the test section was calculated by the integration of the mass flow through the slots, normalized by the total mass flow through the test section which, in turn, is obtained by the integration of the mass flow at the test section entrance, i.e., plane $i = 100$.

A summary of the results for all cases analyzed in the present work is presented in Table 1. Although there was no actual TTP data to compare the results shown in Table 1, these results seemed to be perfectly within the expected range of values for the amount of mass extracted from the tunnel main flow. Moreover, the percentage of mass extracted seems to vary quite linearly with the static pressure ratio at the slots, at least for the particular configuration and tunnel operating condition here analyzed. At this point, the complete implications of this observa-

tion were not fully explored, but the authors expect that further validation of the present calculations will be possible as soon as the TTP becomes operational.

Concluding Remarks

The paper has presented flow simulations relevant to transonic wind tunnel design and operation. Initial tests reproduced some existing tunnel contraction results with the objective of validating the computational code developed. Afterwards, the tunnel test section was included in the computational domain and simulations with both closed and open test section slots were performed. The overall assessment of the results obtained so far is very positive in the sense that all expected flow features have been adequately reproduced by the numerical simulations. The particular tunnel geometry considered models the pilot transonic tunnel, TTP facility, currently under construction at CTA. Experimental results for the flow in this facility should soon be available which will allow further assessment of the quality of the present simulations.

Moreover, the immediate continuation of the present effort will include further grid refinement studies and the inclusion of viscous terms in the formulation. The former will mainly try to assess the effect of smoother, refined meshes in the solution quality and depends, primarily, of the authors getting access to enough computer power to perform the required simulations. The second aspect is a must from the point of view of performing realistic wind tunnel test section evaluations since, clearly, reality is viscous. Therefore, a simulation capability which intends to aid wind tunnel design and operation must include the effect of viscous terms. In particular, boundary layer thickness and boundary layer thickness growth along the tunnel are extremely important parameters for test section flow quality assessment. Furthermore, boundary layer interaction with the flow through the slots is also critical for the efficiency of the ventilated wall concept in transonic tunnels.

Acknowledgments

The authors wish to acknowledge the support of Fundação de Amparo à Pesquisa do Estado de São Paulo, FAPESP, which has provided a Research Scholarship to the first author through the Process No. 96/0565-0. The present work was also partially supported by Conselho Nacional de Desenvolvimento Científico e Tecnológico, CNPq, under the Integrated Project Research Grant No. 522413/96-0.

References

1. Davis, M.W., Gunn, J.A., Herron, R.D., and Kraft, E.M., "Optimum Transonic Wind Tunnel," AIAA 14th Aerodynamic Testing Conference, West Palm Beach, FL, 1986.
2. Fico, N.G.C.R., Jr., Azevedo, J.L.F., and Ortega, M.A., "Use of CFD Methods for Transonic Wind Tunnel Nozzle Selection," ICAS Paper No. 94-2.5.4, *Proceedings of the 19th Congress of the International Council of the Aeronautical Sciences*, Vol. 2, Anaheim, CA, USA, Sept. 1994, pp. 1587-1596.
3. Goethert, B.H., *Transonic Wind Tunnel Testing*, Pergamon Press, New York, 1961.
4. Waitmann, B.A., Reneau, L.R., and Kline, S.J., "Effects of Inlet Conditions on Performance of Two-Dimensional Subsonic Diffusers," *Journal of Basic Engineering*, Vol. 83, Sept. 1961, pp. 349-360.
5. Pulliam, T.H., and Steger, J.L., "Implicit Finite-Difference Simulations of Three-Dimensional Compressible Flow," *AIAA Journal*, Vol. 18, No. 2, Feb. 1980, pp. 159-167.
6. Azevedo, J.L.F., Zdravistch, F., and Silva, A.F.C., "Implementation and Validation of Euler Solvers for Launch Vehicle Flows," *Proceedings of the Fourth International Symposium on Computational Fluid Dynamics*, Vol. I, Davis, CA, Sept. 1991, pp. 42-47.
7. Pulliam, T.H., and Steger, J.L., "Recent Improvements in Efficiency, Accuracy, and Convergence for Implicit Approximate Factorization Algorithms," AIAA Paper No. 85-0360, AIAA 23rd Aerospace Sciences Meeting, Reno, NV, Jan. 1985.
8. Turkel, E., and Vatsa, V,N., "Effect of Artificial Viscosity on Three-Dimensional Flow Solutions," *AIAA Journal*, Vol. 32, No. 1, Jan. 1994, pp. 39-45.
9. Jameson, A., Schmidt, W., and Turkel, E., "Numerical Solution of the Euler Equations by Finite Volume Methods Using Runge-Kutta Time-Stepping Schemes," AIAA Paper 81-1259, AIAA 14th Fluid and Plasma Dynamics Conference, Palo Alto, CA, June 1981.
10. Jameson, A., and Mavriplis, D., "Finite Volume Solution of the Two-Dimensional Euler Equations on a Regular Triangular Mesh," *AIAA Journal*, Vol. 24, No. 4, April 1986, pp. 611-618.
11. Fico, N.G.C.R., Jr., "Simulation of the Flow in the Reentry Flap Region of a Transonic Wind Tunnel," Doctoral Dissertation, Instituto Tecnológico de Aeronáutica, São José dos Campos, SP, Brazil, 1991 (in Portuguese).
12. Azevedo, J.L.F., Fico, N.G.C.R., Jr., Ortega, M.A., and Luna, G.C., "Nozzle Flow Calculations Using the Euler Equations," ICAS Paper 92-4.1.2, *Proceedings of the 18th Congress of the International Council of the Aeronautical Sciences*, Vol. 1, Beijing, China, Sept. 1992, pp. 97-107.
13. MacCormack, R.W., "An Introduction and Review of the Basics of Computational Fluid Dynamics," AIAA Professional Study Series on Computational Fluid Dynamics, Snowmass, Colorado, June 1984.
14. Azevedo, J.L.F., Fico, N.G.C.R., Jr., and Ortega, M.A., "Two-Dimensional and Axisymmetric Nozzle Flow Computations Using the Euler Equations," *J. of the Braz. Soc. Mechanical Sciences*, Vol. 17, No. 2, June 1995, pp. 147-170.